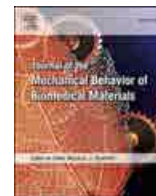


Contents lists available at ScienceDirect

Journal of the Mechanical Behavior of Biomedical Materials

journal homepage: www.elsevier.com/locate/jmbbm

Research Paper

The melanized layer of *Armillaria ostoyae* rhizomorphs: Its protective role and functions

Debora Lyn Porter^{a,*}, Alexander J. Bradshaw^b, Ryan H. Nielsen^a, Pania Newell^a, Bryn T. M. Dentinger^b, Steven E. Naleway^a

^a The University of Utah Department of Mechanical Engineering, USA

^b Natural History Museum of Utah & School of Biological Sciences, University of Utah, USA



ARTICLE INFO

Keywords:

Armillaria ostoyae
Biological materials
Graded porous structure
Finite element model
Biomechanics

ABSTRACT

Armillaria ostoyae (Romagn.) Herink is a highly pathogenic fungus that uses exploratory, cordlike structures called rhizomorphs to seek out new sources of nutrition, posing a parasitic threat to natural stands of trees, orchards, and vineyards. Rhizomorphs are notoriously difficult to destroy, and this resilience is due in large part to a melanized layer that protects the rhizomorph. While this structure has been previously observed, its structural and chemical defenses are yet to be discerned. Research was conducted on both lab-cultured and wild-harvested rhizomorph samples. While both environments produce rhizomorphs, only the wild-harvested rhizomorphs produced the melanized layer, allowing for direct investigation of its structure and properties. Imaging, chemical analysis, mechanical testing, and finite element modeling were used to understand the defense mechanisms provided by the melanized layer. Imaging showed a porous outer layer in both types of rhizomorphs, though the pores were smaller in the harvested melanized layer. This melanized layer contained calcium, which provides chemical defense against both human and natural control methods, but was absent from cultured samples. Nanoindentation resulted in a larger variance of hardness values for cultured rhizomorphs than for wild-harvested. Finite element analysis proved that the smaller pore structure of the melanized porous layer had the best balance between maximum deformation and resulting permanent deformation. These results allow for a better understanding of the defenses of this pathogenic fungus, which may lead to better control methods.

1. Introduction

Members of the fungal genus *Armillaria* are globally distributed phytopathogens that are well known for their ability to infect and kill over 600 types of woody plants (Baumgartner et al., 2011). *Armillaria* is well characterized as a destructive force to both forestry and agricultural settings, with control methods often being only inhibitory to the phytopathogen while also being toxic to the host plant (Aguín et al., 2006). The Georgia peach industry alone experienced more than an estimated \$1.5 million in damages due to *Armillaria* from 2000 to 2002 (Wilson et al., 2020). Generally, individuals of *Armillaria* establish in woodlands and soil substrates by growing vegetatively and producing an extensive network of cordlike structures known as rhizomorphs (Fig. 1a). Rhizomorphs act as long-range exploratory structures that allow an *Armillaria* mycelium, the primary metabolic thallus of the fungus made up of the same hyphae filaments as the rhizomorphs, to seek and infect new host plants. These mycelia and rhizomorph

networks have been found to remain dormant for decades in the environment when live hosts are not available, becoming active again as new hosts return (Baumgartner et al., 2011), (Kromroy et al., 2005; Mihail and Bruhn, 2005; Baumgartner and Rizzo, 2002). Even phenolic fungicides, which have been found to help control other pathogenic fungi (Zabka and Pavela, 2013), can stimulate growth in *Armillaria* (West and Fox, 2002). This resistance to biocontrol and ability to infect new hosts, even after decades of inactivity in the soil, make these *Armillaria* rhizomorphs difficult to eradicate and a blight to both crops and natural stands of plants destroyed by its infection.

Much of the previous and current research on *Armillaria* has focused on its biology and ecology, including taxonomy (Pildain et al., 2010; Anderson and Ullrich, 1979; Anderson and Stasovski, 1992; Coetzee et al., 2003), life cycle (Ullrich and Anderson, 1978; Grillo et al., 2000; Ota et al., 1998; Qin et al., 2007), interactions within the environment (Baumgartner and Rizzo, 2001; Bergemann and Garbelotto, 2006; Proffer, 1987; Schnabel et al., 2006), and potential methods of pest

* Corresponding author.

E-mail address: deboralyn.porter@utah.edu (D.L. Porter).

<https://doi.org/10.1016/j.jmbbm.2021.104934>

Received 6 January 2021; Received in revised form 22 October 2021; Accepted 25 October 2021

Available online 27 October 2021

1751-6161/© 2021 Elsevier Ltd. All rights reserved.

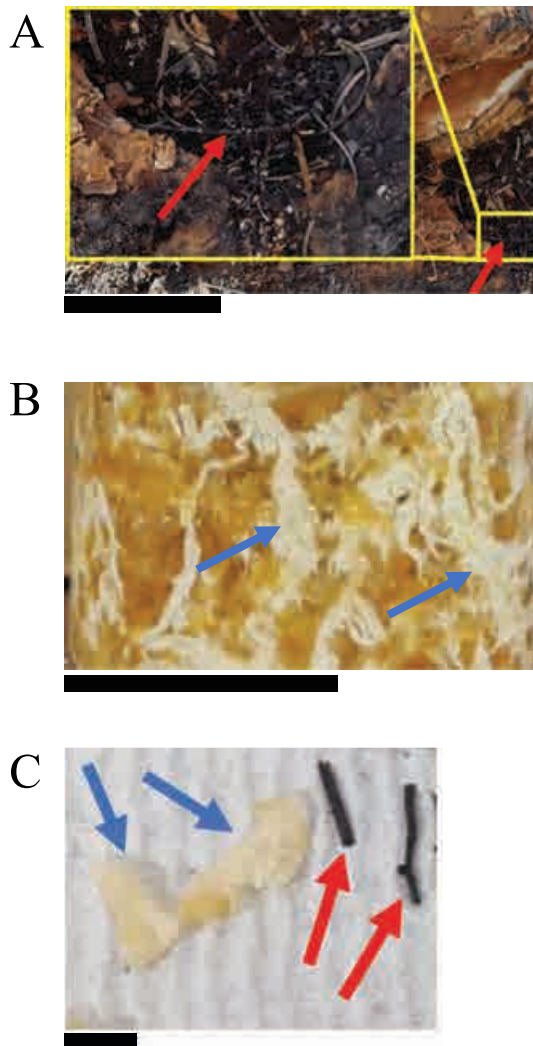


Fig. 1. A: Rhizomorphs found beneath the bark of an infected western white pine tree (*Pinus monticola*). Rhizomorphs are surrounded by a dark, syrup-like liquid; red arrows are placed to point out specific rhizomorphs in the network under the bark. B: Close up image of cultured rhizomorphs, blue arrows are placed to point out specific rhizomorphs, grown in a mason jar. C: Representative images of rhizomorph samples. Cultured rhizomorph samples are on the left, shown with blue arrows, and harvested rhizomorphs are on the right, shown with red arrows. The scale bars all represent 1 cm. (For interpretation of the references to color in this figure legend, the reader is referred to the Web version of this article.)

control (Adaskaveg et al., 1999; Cox and Scherm, 2006; DeLong et al., 2002; Baumgartner and Warnock, 2006). Some previous work has looked into the anatomy of the rhizomorphs in the species *Armillaria gallica* Marxm. & Romagn., which are highly organized microscopically, showing a porous outer layer (Yafetto et al., 2009) as the primary structural element (Yafetto et al., 2009), (Yafetto, 2018). Limited work has been done on the biomechanics of rhizomorph growth (Yafetto et al., 2009; Yafetto, 2018; SanatiNezhad and Geitmann, 2013) in a laboratory setting. However, *Armillaria* rhizomorphs are known to produce a melanized outer layer in their natural environment (Mihail and Bruhn, 2005), (Koch et al., 2017), which is not always present when cultured *in vitro* (see Fig. 1). This melanized layer is believed to provide protection from pests and noxious abiotic conditions (Rizzo et al., 1992), (Cordero and Casadevall, 2017). However, little is known about the mechanisms this melanized layer uses to provide the protection from both mechanical and chemical stresses necessary for the survival of the *Armillaria* rhizomorphs and allow them to be so effective at seeking and infecting

woody plants.

In this work we looked to experimentally and computationally characterize and define the protective structures of *Armillaria* rhizomorphs, with a primary focus on their outer melanized layer. To isolate this layer, we compared the structural, chemical, and mechanical properties between *in vitro* (lab-cultured) and *in vivo* (wild-harvested) rhizomorphs, where cultured rhizomorphs were genetically identical, but lack this melanized layer (as shown in Fig. 1b and c). Studying the structure and mechanical properties of the melanized layer fills a gap in the knowledge of how this highly pathogenic fungus is able to survive and continue to infect new hosts. This could also provide a direction for research into weakening *Armillaria* rhizomorphs in a way that would slow or stop the spread of this highly infectious and damaging parasite.

2. Materials and methods

2.1. *In vivo* harvested rhizomorph collection

In vivo harvested samples were collected from the Malheur National Forest, OR, USA, which is the site of a number of large *Armillaria* genets (genetic individuals) including the world's largest genet known as the "Humongous Fungus." *Armillaria ostoyae* samples were taken from Genet E of the known Malheur clusters (Ferguson et al., 2003). Rhizomorphs were found by looking for symptomatic trees, characterized by dying needles and surrounded by other dying trees. The outer layer of bark was cut into using a hatchet, then peeled from the root collar down into the roots (Fig. 1a) (Ferguson et al., 2003), according to the procedure set forth by the Malheur Forest Service forest pathologist. Rhizomorphs were located beneath the bark and pulled up from the roots and soil. Collected rhizomorphs were placed in damp paper towels and kept in paper bags in either an insulated cooler (during transit to the lab) or a refrigerator (while in the lab). Rhizomorphs were kept hydrated until testing by keeping the paper towels that they were wrapped in wet, to reduce the risk of drying out and breaking. These samples are referred to henceforth as "harvested rhizomorphs."

2.2. *In vitro* cultured rhizomorph culturing

In vitro culturing was performed by following the procedure established by Sipos et al. (Sipos, 2017) for generating sporocarps, with alteration to the growth jar apparatus. The growth jar apparatus was created by puncturing a 2 mm diameter hole in the top of a ~1000 mL wide mouth mason jar (Ball Corporation, Broomfield, CO, USA) that was then filled with tightly wound PolyFil polyester fibers (Fairfield Processing Corporation, Danbury, CT, USA). This was done to provide airflow to the growing culture without compromising the sterility of the jar during the growth process. Jars were initially autoclaved for 30 min on a dry cycle before growth media was added. Growth media consisted of 30 g of brown rice, 20 g of pine shavings, 500 mL of water, and 100 g of finely chopped oranges with the peel. This mixture was then autoclaved for 30 min on liquid cycle, then layered with ~2.5 cm of homogenized tomatoes, and autoclaved for 30 min on a liquid cycle. Agar plugs of cultured *Armillaria* mycelium previously collected from Genet E (Ferguson et al., 2003), the same genet as the harvested rhizomorphs, were then inoculated into the jars within a sterile laminar flow hood and allowed to grow and colonize the entirety of the jar at room temperature using a light cycle of 12 h on then 12 h off (see Fig. 1b), for no fewer than 4 weeks of incubation (Sipos, 2017). These samples are referred to henceforth as "cultured rhizomorphs."

2.3. Structural imaging

Sections approximately 8 mm in length were cut from different sections of both the harvested and cultured rhizomorphs to make imaging samples (Fig. 1c). These imaging samples were roughly a hollow cylinder in geometry and were prepared using previously established

procedures (Yafetto et al., 2009). Samples were first preserved by placing them into a fixative (2.5% glutaraldehyde/2.5% formaldehyde) for 2 h then rinsing them twice with a 0.1 M sodium cacodylate solution for 10 min per rinse. The imaging samples were then serially dehydrated in ethanol (with 10 min treatments at 50%, 70%, 95%, 95%, 100%, 100%, 100% ethanol) before being freeze fractured (using liquid nitrogen) and freeze-dried using a Labconco FreeZone 1 freeze drier (Kansas City, MO, USA) for a minimum of 12 h to ensure all fluid was removed. Following the freeze-drying procedure, samples were affixed to aluminum sample holders using carbon tape and coated with ~15 nm of gold palladium. Images were taken in an FEI Quanta 600FE-ESEM scanning electron microscope (Hillsboro, OR, USA) at an accelerating voltage of 5 kV and spot size of 3 nm. Images of the exterior surfaces and transverse cross-sections of both cultured and harvested rhizomorphs were taken. In each case, three images were taken of each section (surface and transverse cross-section) from three harvested and three cultured samples.

The SEM images of the harvested and cultured rhizomorph cross-sections were analyzed using ImageJ. Three images each of cultured and harvested samples were used for calculating the pore sizes and degree of porosity. Pore sizes were measured by taking the images of the porous layer sections at 500 times magnification, isolating the pores with ImageJ and analyzing the pore size of all the visible pores. Pores were separated into three categories, based on size using R software (The R Foundation): small ($0\text{--}10\ \mu\text{m}^2$), medium ($10\text{--}20\ \mu\text{m}^2$), and large (larger than $20\ \mu\text{m}^2$). In each case, no fewer than 122 pores were measured from each sample. The average porosity for each image was measured by taking three representative sections from each image of the porous layer at 500 times magnification and using ImageJ to calculate the percent area of the sample made up of pores. Using these averages, the average porosity for each type of sample (i.e., cultured and harvested) was calculated. Using ImageJ, porous layers were divided into three sections: the outside, middle, and inside third of the layer, respectively, as seen in Fig. 2. The size of the pores in each section were measured using ImageJ.

2.4. Chemical composition

While samples were in the SEM, energy dispersive x-ray spectroscopy (EDS) was performed using APEX EDS Software (EDAX Inc., Mahwah, NJ, USA). Chemical composition and elemental maps, as found using the EDS software, were completed on the outer surface and transverse cross section of three harvested and three cultured imaging samples. EDS was completed using an accelerating voltage of 20 kV and a spot size of 5.0 nm. Image outputs were adjusted to leave out elements present due to fixing (hydrogen from glutaraldehyde and formaldehyde) and coating the imaging samples (gold and palladium).

2.5. Mechanical testing

Sections approximately 3.5 mm in length were taken from the larger rhizomorph samples to make three harvested and three cultured mechanical testing samples (similar to those seen in Fig. 1c). To ensure similar testing conditions, mechanical testing samples were placed on paper towels to dehydrate for 30 min. After samples were dehydrated, they were placed on 15 mm diameter Specimen Discs (Ted Pella, Redding, CA, USA) with cyanoacrylate glue. Nanoindentation on the outside surface of the mechanical testing samples was performed using a Hysitron TI Premier Nano indenter system (Hysitron Inc., Minneapolis, MN, USA) with a Berkovich tip probe. A trapezoidal load function with a maximum load of $500\ \mu\text{N}$ was used. Each mechanical testing sample was indented in eight locations on the sample to allow for a minimum of 5 useable data sets, should some of the indentations slip or otherwise provide unusable data.

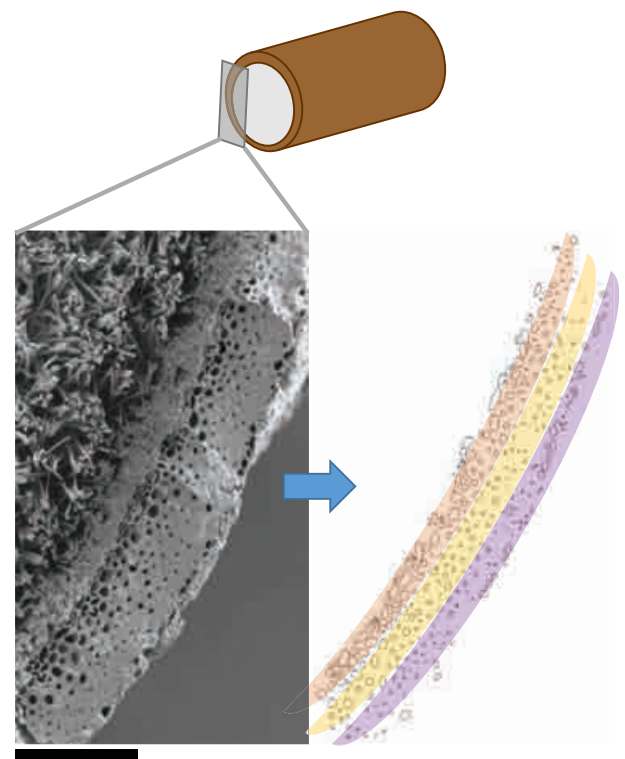


Fig. 2. Representative porous layer of a harvested rhizomorph (left) and pores broken into sections: outside (purple), middle (yellow), and inside (orange) sections. The scale bar represents $50\ \mu\text{m}$. (For interpretation of the references to color in this figure legend, the reader is referred to the Web version of this article.)

2.6. Computational modeling

2.6.1. Finite element model

A 2D plane-strain Finite Element (FE) model of the nanoindentation test was developed using Mechanical ANSYS Parametric Design Language (MAPDL) in commercial ANSYS software (Ansys, Inc., Canonsburg, PA, USA). A cross section depicting the ordered 3-section (i.e., outside, middle, and inside sections) pore structure of the harvested rhizomorph samples was created to perform a parametric study of the effect of the porosity on the deformation under nanoindentation (Fig. 3).

2.6.2. Geometry

The Berkovich tip probe, used in the nanoindentation tests, was approximated by a 2D wedge with a 65.27° half angle (Hysitron, 2016). The output data of the physical nanoindentation tests was 30% greater than what would be expected by using a perfect Berkovich probe tip for a given contact depth (Oliver and Pharr, 1992), suggesting tip wear. To account for this wear, which can affect the radial size of the tip (Torres-Torres et al., 2010), (Lofaj and Németh, 2017), a $1.5\ \mu\text{m}$ tip radius was used for modeling rather than the probe tip's $150\ \text{nm}$ nominal value (Hysitron, 2015) (Fig. 3a).

The geometry of the outer layer of the rhizomorph (the melanized layer for harvested rhizomorphs and outer layer for cultured rhizomorphs) was approximated as a $100.1\ \mu\text{m}$ by $44.1\ \mu\text{m}$ rectangular cross section based on the SEM images and measurements. For consistency across the whole rhizomorph model and inspired by the SEM images, all pores were modeled as ellipses with a major to minor axis ratio of 2:1 and sized to the appropriate area to capture the correct area of pores and porosity of the porous layer. Pores were separated into 3 sections: inside, middle and outside (Fig. 3), to match the pore structure, as depicted in SEM images (see Fig. 2) of the harvested rhizomorph samples.

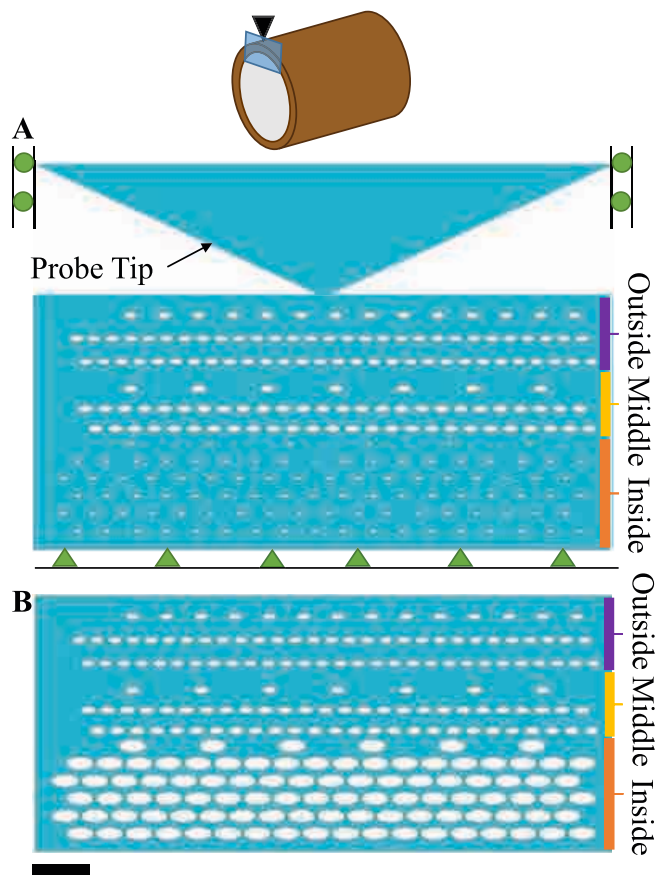


Fig. 3. Geometry of the finite element model. Note that the pores in the outside and middle sections are held at the average pore size for each respective section in both A and B. The inside pores are varied from a factor of 0.14 (A) to 1.4 (B), where a factor of 1 is equal to the average size of the pores in the harvested rhizomorph. Boundary conditions are shown in A: a zero-horizontal displacement along the top of the indenter, and a zero-displacement boundary condition along the bottom of the inside layer. The scale bar represents 100 μm .

2.6.3. Material model

The material model used for the diamond Berkovich probe tip used a Young's modulus of 1140 GPa and a Poisson's ratio of 0.07 (as described in the Hysitron probe part specifications). The rhizomorph material was modeled as a bilinear elastic-plastic with a von Mises stress yield initiation assumption. The reduced Young's modulus was found by analyzing the average unloading curve of the load-displacement data obtained from nanoindentation of the harvested rhizomorph mechanical testing samples, using a previously established technique (Oliver and Pharr, 1992). Young's modulus was calculated using the reduced modulus and the material properties of the probe tip (Oliver and Pharr, 1992). Because the primary constituent of the rhizomorph cells is chitin, a Poisson's ratio of 0.25 was used based on previous experiments performed on chitin fibers (Wan and Hao, 2020). An appropriate yield stress ($\sigma_y = 28$ MPa) was iteratively determined by validating the plastic deformation of the model to the experimental data.

2.6.4. Mesh

The model was meshed with 40572 eight- and six-node quadratic PLANE183 plane-strain elements. The rhizomorph and probe tip contact surfaces were refined to 1/9th of the surrounding element size. The top of the outside section of the porous media was meshed with TARGET169 target elements while the tip of the indenter was meshed with CONTA175 contact elements. A convergence study was conducted to ensure the results would not be mesh sensitive.

2.6.5. Boundary and loading conditions

A zero-displacement boundary condition was prescribed along the inside surface of the rhizomorph model, while a zero-horizontal displacement boundary condition was prescribed along the top of the indenter (see Fig. 3a). A trapezoidal load function with a maximum load of 500 μN (to match the experimental mechanical testing) was applied vertically along the top boundary of the indenter. A bonded contact condition was applied between the probe tip and rhizomorph contact surfaces.

Porosity was varied using a factor of the average pore size, varying between 0.14 and 1.4 times the average pore area of each section, with a factor of 1 equal to the average pore size determined from the harvested rhizomorphs. This range was determined by using the average pore area and interquartile range to capture the majority (no less than 75%) of pore sizes without skewing the data with outliers. Four scenarios were investigated to determine the impact of varying the pore size: (1) varying the average pore size of all of the sections simultaneously and by the same factor, (2) varying only the pores of the inside section, (3) varying only the pores of the middle section, and (4) varying only the pores of the outside section. In the scenarios in which only one section's pores were varied, all other sections were held constant at a factor of 1 (as shown for the case of varying only the pores of the inside section between Fig. 3a and b). This was done to analyze the impact of pore size and resulting porosity in the three sections of the rhizomorph under constant mechanical loading. For each scenario, a load-displacement curve was generated. The plastic deformation for each scenario was then calculated by taking the difference between the final displacement after unloading and initial displacement under the same load.

2.7. Generation of ITS barcode for cultured rhizomorphs

To ensure that the cultured rhizomorphs were genetically the same (of the same species) as the harvested rhizomorphs, DNA was extracted from cultured samples by harvesting ~ 10 mg of mycelial tissue that was grown on 2% malt agar plates and grinding it in the presence of liquid nitrogen using a mortar and pestle. Genomic DNA was extracted from the resulting pulverized tissue using Extract-N-AmpTM Tissue PCR Kit (Sigma-Aldrich, St. Louis, MO, USA). Polymerase chain reaction (PCR) was performed using primers ITS1F and ITS4 (White et al., 1990), (Gardes and Bruns, 1993) for targeted amplification of the nuclear ribosomal internal transcribed spacers (ITS), which is the official DNA barcode region for Fungi (Dentinger et al., 2011) and is the primary marker for species identification in *Armillaria* (Coetzee et al., 2018). PCR thermocycler settings and conditions were used as outlined in previous work (Schochet et al., 2012), and confirmed by agarose gel-electrophoresis. Amplified samples were then purified using ExoSAP-ITTM PCR Product Cleanup Reagent (Thermo Fisher Scientific, Waltham, MA, USA). Forward and reverse strand Sanger sequencing of clean samples was performed at the DNA Sequencing Core Facility at the University of Utah.

2.8. Statistical analysis

Analysis of variance (ANOVA) and Tukey's honest significant difference (HSD) tests were used to determine significance, as has been done for similar projects (Wan and Hao, 2020), (Yu et al., 2008). For each measured property (i.e., proportion of pore sizes, pore sizes in different sections of the porous layer, porosity, hardness), a one-way ANOVA test was performed using R software. Except for comparing the porosity between sections, the factors considered in statistical testing were the type of rhizomorph sample: cultured or harvested. In the case of determining significance in the porosity between sections, each of the sections were the factors of interest: the inside, middle, and outside section. When statistical significance was determined by the one-way ANOVA and pairwise comparisons were necessary, a Tukey's HSD test was used. A significance level of $\alpha = 0.05$ was used for all tests

to establish statistically significant differences.

3. Results and discussion

3.1. Species identification of isolates

Species identification in *Armillaria* is difficult and often ambiguous (Ferguson et al., 2003). In order to reduce the chances of property variance being a result of a difference in species, harvested rhizomorphs were collected from the same known *Armillaria* Genet ("Genet E"), where the *Armillaria* hyphae for the cultured samples were collected. In addition to choosing a previously studied site, field identification of infected hosts and direct isolation of rhizomorphs was performed according to commonly used USDA guidelines (Sipos, 2017). Genet E, studied by Ferguson et al. (Ferguson et al., 2003), was shown to be a genetically identical single organism that spread across tens of thousands of square meters of land (Baumgartner and Warnock, 2006). In that study, Ferguson et al. used restriction fragment length polymorphism (RFLP) to initially detect the species of Genet E, which was determined to be *Armillaria ostoyae*. The current study is possibly the first to report generation of the ITS DNA barcode for Genet E. This barcode sequence, when compared to the GenBank sequences, exhibits a 90.27% percent sequence identity with the top basic local alignment search tool (BLAST) hit, which was labeled as *Armillaria* cf. *ostoyae* (Accession number: AY228342.1). This percent sequence identity is lower than expected for conspecifics in fungi, which is generally considered a match with percent identity above 95%–97% (Schochet et al., 2012), (Yahr et al., 2016), although intragenomic variation may exceed this interspecific threshold (Tremble et al., 2020). This finding may indicate greater species diversity within the *Armillaria* genus; however, for the purposes of the current study, these results indicate that both the harvested and cultured rhizomorphs come from the same organism, meaning any differences in structure, behavior, or properties was not a result of genetic differences.

3.2. Rhizomorph structure

Similar to previous work on other *Armillaria* species, the current rhizomorph samples had a porous layer (Fig. 4a–b) (Yafetto et al., 2009), which was the melanized layer for the harvested rhizomorphs and the outer layer for the cultured rhizomorphs. Pores showed a general decrease in size moving radially outward in the porous layer (Fig. 4a and b,5). Of note, there was a statistically significant difference in the sizes of the pores of each section (inside, middle, and outside) between the cultured and harvested rhizomorph samples. The significance of all pairwise comparisons can be seen in Table 1. No statistically significant difference was found between the medium sized pores, but there was a statistically significant difference (with $p = 0.00002$) between the proportion of large pores found in the cultured and harvested rhizomorphs, as well as with the small pores ($p = 0.008$) (see Fig. 6), indicating that cultured rhizomorphs have larger pores overall. Cultured samples showed greater porosity in their porous layers, with a statistically significant difference ($p = 0.036$) in the porosity between the cultured (mean value of 40.76 and a standard deviation of 17.72) and the harvested (mean value of 25.52 and a standard deviation of 9.78) rhizomorphs. These results demonstrate that not only is the melanized layer of the harvested rhizomorphs less porous with smaller pores than the outside section of the cultured rhizomorphs, but also that the melanized layer of the harvested rhizomorphs have smaller pores overall.

The surface images of the rhizomorphs (Fig. 4c and d) showed that the surface of the melanized layer in the harvested rhizomorphs had a smoother surface, in which the fused hyphal cords showed a more axial orientation across the surface (Fig. 4c). The cultured samples had an outer surface that appeared loosely woven and fused together, with visible gaps in the surface (Fig. 4d). The smoother surface of the harvested rhizomorph samples likely also helped to create a more uniform

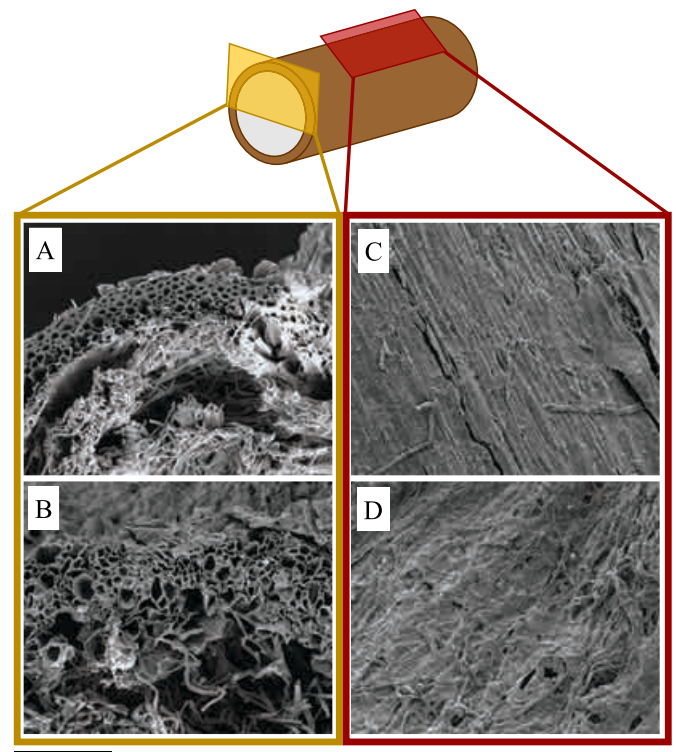


Fig. 4. Representative images of porous layer of rhizomorphs of (A) harvested, and (B) cultured rhizomorphs. (C, D) Representative images of outer surfaces of (C) harvested and (D) cultured rhizomorphs. The scale bars represent 50 μm .

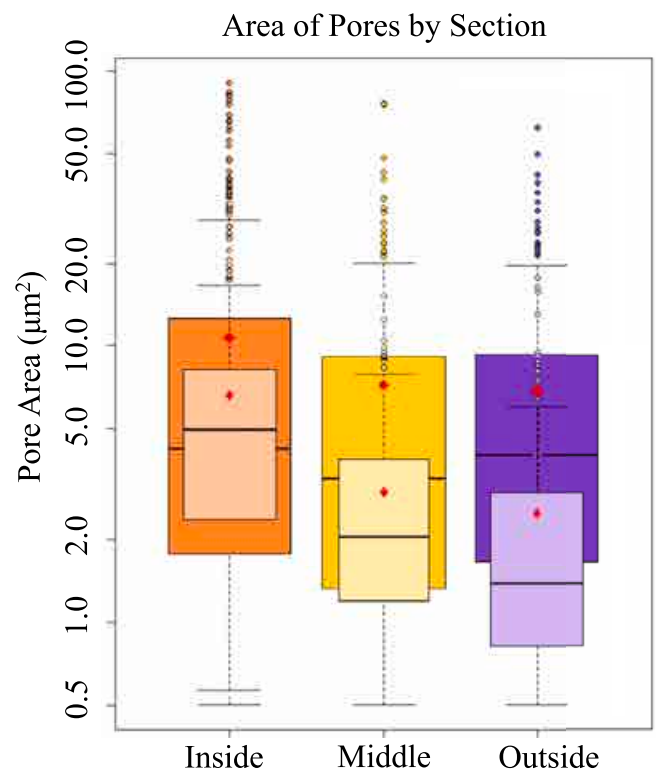


Fig. 5. Pore area by section of the outer layer (inside, middle, and outside). Darker plots represent cultured rhizomorphs samples and lighter plots represent harvested rhizomorphs samples. Red diamonds represent mean values. (For interpretation of the references to color in this figure legend, the reader is referred to the Web version of this article.)

Table 1

Statistical significance, including p values, of the area of the pores in the inside, middle, and outside sections of the porous layer for the cultured and harvested rhizomorph samples. Pairwise comparisons were made between the same sections of the cultured and harvested rhizomorphs samples, as well as between the different sections in both the cultured and harvested rhizomorph samples. P values less than the established significance level ($\alpha = 0.05$) are bolded.

Separation of Factors	Pairwise Comparison	p value
Cultured	Middle-Inside	1.28e-3
	Outside-Inside	3.95e-5
	Outside-Middle	0.95
Harvested	Middle-Inside	$< 10^{-15}$
	Outside-Inside	$< 10^{-15}$
	Outside-Middle	0.54
Inside	Harvested-Cultured	3.34e-5
Middle	Harvested-Cultured	1.47e-7
Outside	Harvested-Cultured	2.69e-14

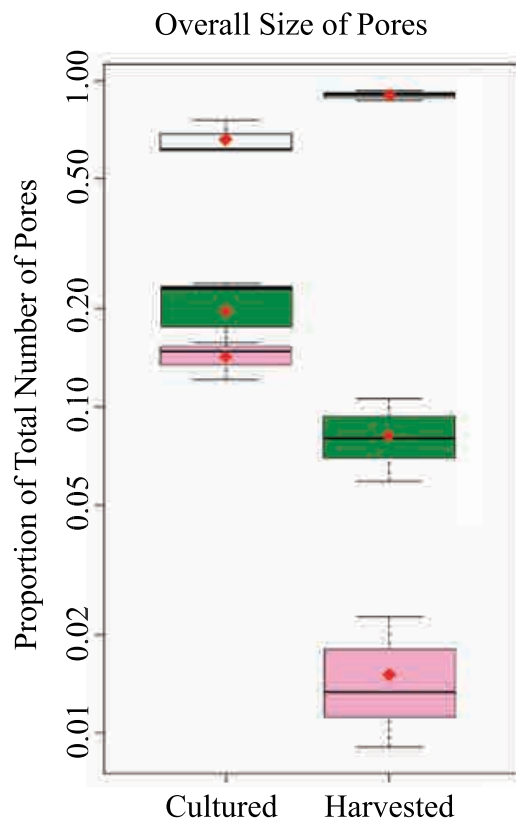


Fig. 6. Overall size of rhizomorph pores. Combined boxplots for large (pink boxes), medium (green boxes), and small (white boxes) pores for cultured and harvested rhizomorphs. Red diamonds represent mean values. (For interpretation of the references to color in this figure legend, the reader is referred to the Web version of this article.)

structural surface. The lack of uniformity in the cultured rhizomorph samples may provide advantageous properties to certain sections while simultaneously allowing for natural weak spots in others. Under stress, it is the weak spots that play the more significant role in failure, and better define the failure properties of a material.

Previous work has hypothesized that the pores could play a part in translocation along the length of the rhizomorph (Yafetto et al., 2009). If the pores are used in translocation, smaller pores on the outside of the rhizomorph suggests that nutrients and gases are transported more towards the center, where translocation is less restricted by small pore size. Gradient structures are also known to affect mechanical properties, such as improving toughness and resistance to wear (Naleway et al.,

2015). Harvested rhizomorphs, which have the melanized layer that is a denser porous layer than cultured rhizomorphs, could take more surface damage with less risk of damaging their ability to transport essential nutrients. This damage resistant structure protects the rhizomorphs and could play a key role in keeping rhizomorphs dormant instead of dying when nutrition may be limited. The inner porous core of the rhizomorphs may also improve the overall toughness of the structure, such as in the case with arapaima fish scales, whose different layers with their distinct properties increase their effectiveness as an armor (Yanget al., 2014).

One biocontrol method used to stop or slow the spread of *Armillaria* employs *Trichoderma*, an antagonistic fungus that attacks and outcompetes the pathogenic *Armillaria* to a point where its pathogenic effects are not as devastating on the host plant (Pellegrini et al., 2014; Munnecke, 1981; Munnecke, 1973). Having a denser outer surface, as is the case with the harvested rhizomorphs, would provide a better protection against bio-controls than a porous surface, as seen in the cultured samples. Therefore, these results demonstrate that the outer melanized porous layer of the harvested rhizomorphs provides protection against predators or competitors while maintaining essential functions like translocation of nutrients.

3.3. Chemical composition

Table 2 shows the average values of the most abundant elements present in the rhizomorphs, as detected using EDS. The most abundant elements were carbon (C) and oxygen (O) in both the harvested and cultured samples. Trace elements, elements with less than three weight percent detected, were found in both types of rhizomorphs. However, calcium was consistently present in the harvested rhizomorphs in larger amounts (about five weight percent), but was absent from the cultured rhizomorphs. Fig. 7 shows EDS mapping images of cultured and harvested rhizomorph samples. These images show an even distribution of carbon and oxygen, as is expected from organic material. However, the harvested samples showed an even distribution of calcium in the porous layer (Fig. 7a) and on the outer surface (Fig. 7c), though no significant amount of calcium was detected in the interior of the rhizomorph. There was no similar distribution of calcium in the cultured samples (Fig. 7b, d).

The melanized layer in the harvested rhizomorphs is distinctive due to its darker pigmentation, but also from the presence of calcium. Fungal melanins are known to provide a host of benefits to the fungi that produce them, including metal binding (Cordero and Casadevall, 2017); some melanized fungi are able to absorb metal ions, such as Ca^{2+} , from their environment (Fogarty and Tobin, 1996). This metal binding ability can provide increased chemical protection from environmental hazards, such as heavy metal toxicity (Munnecke, 1973), while also providing a precursor to chemical defenses from possible predation or defensive attacks from potential hosts. The presence of calcium in the outer layer of the harvested rhizomorphs suggests the binding of melanins with calcium ions in the soil to provide greater chemical protection while seeking new hosts. The cultured, non-melanized rhizomorphs had no such environmentally derived benefit. The elemental makeup of the melanized layer of the harvested rhizomorphs had approximately five

Table 2

Most abundant elements in cultured and harvested rhizomorphs found using energy dispersive x-ray spectroscopy. Trace elements (<3 wt % each) are not individually named.

Element	Weight Percent (%): Mean (Standard Dev.)	
	Cultured Rhizomorphs	Harvested Rhizomorphs
Carbon (C)	45.63 (0.02)	47.77 (2.35)
Oxygen (O)	53.65 (0.84)	43.01 (0.65)
Calcium (Ca)	–	5.09 (1.24)
Trace Elements (remaining %)	0.72	4.13

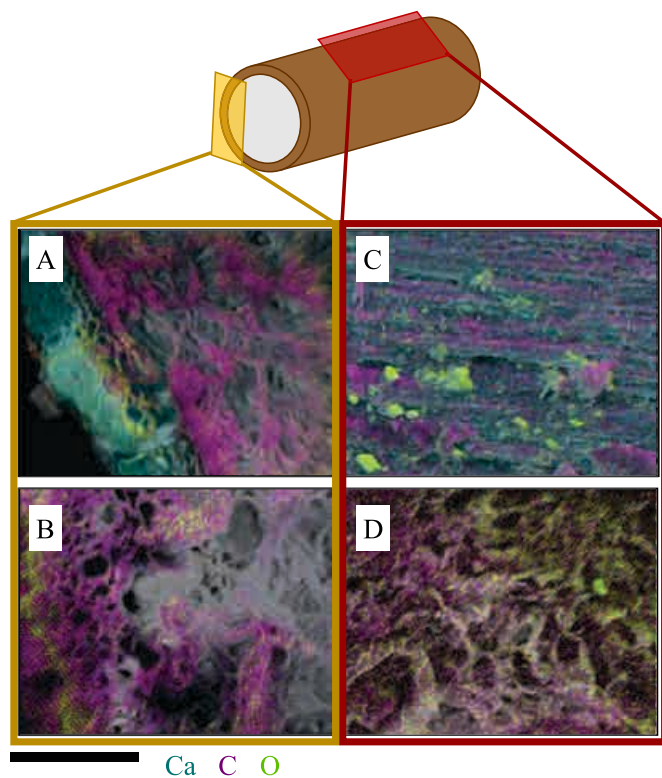


Fig. 7. EDS chemical composition maps. A: Transverse cross section of a harvested rhizomorph sample. B: Transverse cross section of a cultured rhizomorph sample. C: Surface of a harvested rhizomorph sample. D: Surface of a cultured rhizomorph sample. Teal represents calcium, purple represents carbon, and green represents oxygen. The scale bar represents 50 μm . (For interpretation of the references to color in this figure legend, the reader is referred to the Web version of this article.)

weight percent of calcium, suggesting that this addition of calcium adds a layer of chemical protection, rather than bolstering the mechanical defenses. This was further explored in examining mechanical properties of the rhizomorphs.

Insight into the role of the increased calcium in the harvested rhizomorphs can come from looking at an analogous system. Studies in ectomycorrhizal (EM) fungi, which are also known to produce rhizomorphs, form beneficial interactions with a host through the root system and show significant concentrations of calcium within their mycelium (Wallander et al., 2003). This calcium often manifests on the surface of rhizomorphs, or other surface mycelia, in the form of calcium oxalate crystals, and is believed to be a protection from predation and microbial attack (Wallander et al., 2003), (Whitney and Arnott, 1987). While *Armillaria* has a parasitic/saprotrophic lifestyle, infecting a host through the root system, rhizomorphs likely face similar attacks, and would benefit from similar calcium-based defenses.

Beyond the protection from predation, these calcium-based protections also help in invading new hosts. As the rhizomorphs invade a new host, the host plant will employ defense mechanisms. These mechanisms can include the production of areas with an increased pH and antimicrobial properties (Nagy et al., 2012). White rot fungi, such as *Armillaria*, use oxalic acid to fight these defenses. The oxalic acid and creation of calcium oxalate crystals allows the invading, pathogenic rhizomorphs to lower the pH of the defending host (Nagy et al., 2012). Thus, the melanization of the harvested rhizomorphs combined with the added defenses of the calcium present, provides the rhizomorph with both better defense and greater virulence.

3.4. Mechanical testing

Nanoindentation showed that both cultured and harvested samples had a similar mean hardness value of ~ 242 MPa (see Figs. 8 and 9). However, the cultured samples had a large variation in hardness (standard deviation of 301.29 MPa compared to 72.47 MPa for the harvested samples) and a much lower median when compared to the harvested samples (87.06 MPa and 263.73 MPa, respectively), with a minimum value nearly an order of magnitude smaller than the harvested samples (4.03 MPa and 35.20 MPa, respectively). There was no statistically significant difference between the hardness of the outer surface of the cultured and the harvested rhizomorphs ($p = 0.994$). These hardness values were compared with previous literature that employed similar mechanical testing procedures for biological structures with similar basic constituent material as the rhizomorphs (chitin). The median value of hardness for the harvested rhizomorph was similar to that of locust cuticle (mean of 260 MPa) (Wan and Hao, 2020) and of the internal layers of lobster carapace (mean of 230 MPa) (Erko et al., 2013) suggesting that the rhizomorph is able to provide similar defensive capabilities as the exoskeletons of those organisms. The similarity of the hardness values of the surfaces of the rhizomorph samples to other chitin based materials confirms that the addition of any calcium or calcium oxalate crystals (which have a measured hardness value of approximately 530 MPa using similar indentation methods) (Nicolás-Bermúdez et al., 2018) may not significantly enhance the mechanical properties of the rhizomorphs.

Because the nanoindentation was performed on dehydrated samples, the hardness values were more valuable as a point of comparison between the harvested and cultured samples rather than an estimation of *in vivo* properties. The large standard deviation value as well as the difference between the mean value and the median value of the hardness of the cultured samples shows a great amount of variation where a few measurements skew the overall average of the cultured samples. The hardness values of the harvested rhizomorphs, which were taken from the melanized layer showed less variation.

To infect new hosts, rhizomorphs must maintain mechanical resistance. This resistance is especially important in the infection of new hosts. Rhizomorphs use a combination of enzymes and mechanical force to reduce the integrity of the host's protective layers and then penetrate through them to infect the new host (Baumgartner et al., 2011), (Yafetto

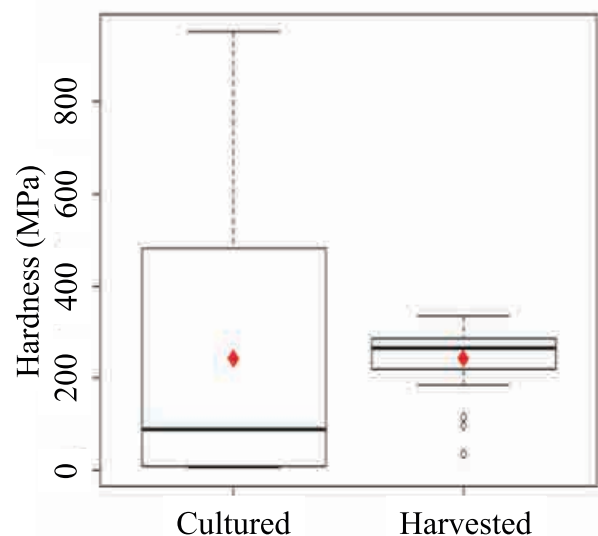


Fig. 8. Boxplot of the hardness of the dehydrated surfaces of the cultured and harvested rhizomorphs. The red diamonds represent the mean value of each set of data. (For interpretation of the references to color in this figure legend, the reader is referred to the Web version of this article.)

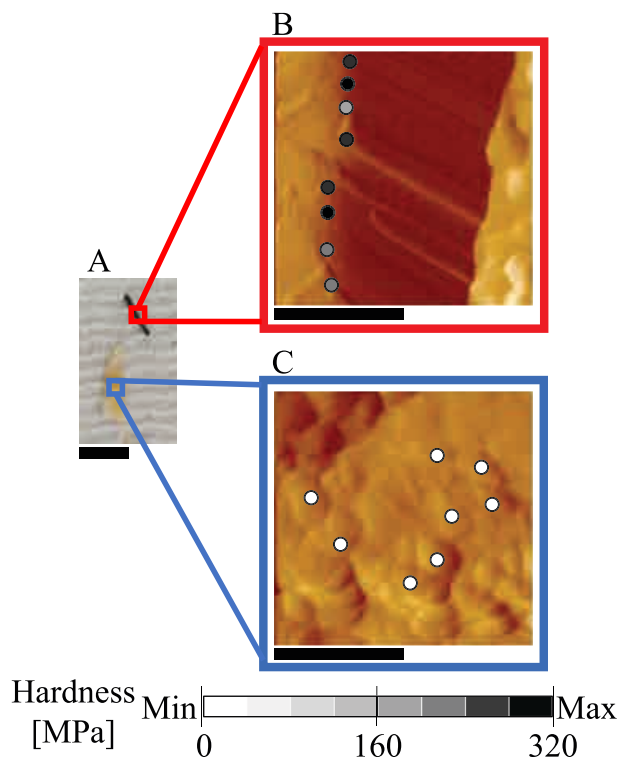


Fig. 9. Distribution of hardness of mechanical testing rhizomorph samples. A: Mechanical testing samples: harvested sample (top), and cultured sample (bottom). B, C: Atomic force microscopy image of the harvested (B) and cultured (C) rhizomorph mechanical testing samples. Circles represent where indents were made, with darker shades representing larger hardness values and lighter shades representing smaller hardness values. Scale bars represents 1 cm (A) and 5 μm (B, C). (For interpretation of the references to color in this figure legend, the reader is referred to the Web version of this article.)

et al., 2009). Both during the exploration for and infection of a new host, rhizomorphs must maintain some structural integrity to propagate. This structural integrity also ensures that the rhizomorphs can efficiently transfer nutrients from the host and withstand attacks from microphagous animals and microparasites. Whether under attack from a host's defenses, microbial attack, or predation, the mechanically weakest point of the rhizomorph will be the point of failure. The smaller minimum hardness value of the cultured samples indicates that cultured rhizomorphs have natural weak spots more susceptible to attack than the weakest points of the harvested rhizomorphs. The non-uniform, loosely woven nature of the cultured sample surface provides such weak spots. This kind of outer surface has a greater number of weak points than the uniform, tightly fused protective surface of the melanized layer in the harvested rhizomorphs. This mechanical resistance may also benefit from the added chemical protection provided by the addition of calcium in the melanized layer. Treatments designed to limit or control rhizomorph growth, by weakening rhizomorph protections would have to first overcome the chemical defenses and then the mechanical defenses. In harvested rhizomorphs, there is a combination of chemical and mechanical defenses which is not present in the cultured rhizomorphs, whose spaces between fused hyphal cords may allow damage to occur more easily to the essential internal structures or functions of the rhizomorph. The uniformity of the melanized layer (as seen in Fig. 4c) of the harvested rhizomorphs also likely contributes to the smaller variance of the measured hardness values, providing more consistent protection from potential attack.

3.5. Computational analysis

Simulations using finite element models showed a strong dependence in the mechanical behavior of the porous layer of the rhizomorph based on the pore size and resulting porosity, as demonstrated by the load-displacement curves shown in Fig. 10. The simulated values align with the experimental nanoindentation data when the factor of average pore size is one, which indicates that the model is a good representation of the average harvested rhizomorph. The two scenarios in which the pores located in the outside section of the porous layer were varied (Fig. 10a and d, respectively) show the most variation in the load-displacement behavior as the pore size changes. The variation of the pore sizes within the inside layer showed less variation in the load-displacement behavior (Fig. 10b). Varying the pores in only the middle section, however, produced very little effect in how the porous layer, as a whole, deformed under the given loading conditions (Fig. 10c).

The maximum displacement of the indenter probe tip during loading was consistently greater when the size of the pores was increased (see Fig. 11a). Varying all pore sizes had the greatest effect on the maximum displacement, changing by 0.332 μm from the minimum (0.14) to the maximum (1.4) factors of the average pore size. The next largest difference came from varying the outside pores, with a difference of 0.2614 μm . The difference in the inside and middle pores was less pronounced, 0.157 μm and 0.0483 μm respectively.

Decreasing the size of the pores in any section of the porous layer had little effect on the plastic deformation following nanoindentation. As seen in Fig. 11b, from a factor of average pore size from 0.14 to 1, all the curves showed similar behavior, with the plastic deformation remaining within a 0.01 μm range. It should be noted that there was no increase in plastic deformation when the pore sizes of the middle and inside sections were increased. Enlarging the average size of the outside pores by a factor of 1.4 resulted in an increase of 0.1506 μm in plastic deformation,

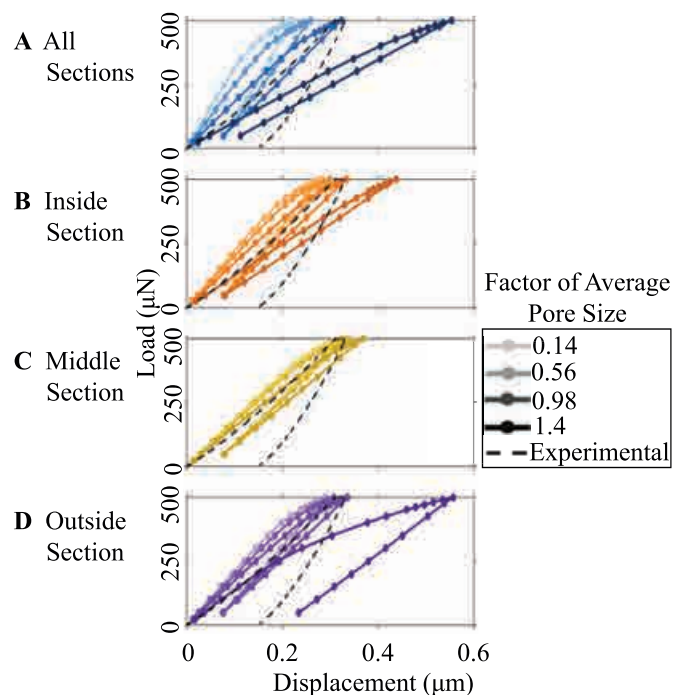


Fig. 10. Load-displacement curves derived from simulating nanoindentation of a harvested rhizomorph with a finite element model graphed with a representative experimental data curve. Each different colored line refers to a factor of the average pore size when varying the pores in the various sections of the porous layer of the rhizomorph. A: Varying all pores. B: Varying inside pores. C: Varying middle pores. D: Varying outside pores. Factors of average pore size shown were selected to have four evenly spaced factors between and including the minimum and maximum factors.

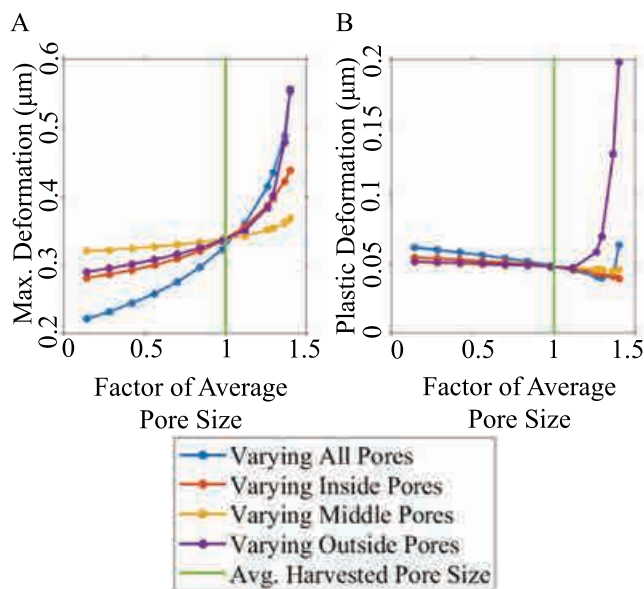


Fig. 11. A: Maximum displacement of probe tip versus the factor of the average pore size when varying each of the sections of the finite element model. B: Plastic displacement versus the factor of the average pore size when varying each of the sections of the finite element model. The plastic deformation is the difference between the final displacement after unloading and initial displacement under the same load. (Fig. 10).

more than tripling the plastic deformation present with average sized pores.

Simulations showed that changing the size of the pores nearest to indentation (outside section) had the greatest effect on the overall mechanical response of the protective porous layer. Maintaining smaller pores in the outside section of this layer offered greater protections to the rhizomorph and its functions against external loading. As shown in Fig. 5 and Table 1, the pores in the outside section of the porous layer are significantly smaller in the melanized layer of the harvested rhizomorphs than in the porous layer of the cultured rhizomorph. The factor of average pore size of the pores in the cultured rhizomorph is 2.21 times as large as the average size of the pores in the harvested rhizomorph. This factor is greater than what is shown in Fig. 11, suggesting that the porous layer of cultured rhizomorphs would experience greater plastic deformation than harvested rhizomorphs under similar loading conditions. Keeping other parameters the same, the differences in structure between the harvested and cultured rhizomorphs, which are symbolic of the melanized layer, provide a better protection in the harvested rhizomorphs against deformation and damage under external loads.

Plastic deformation occurs as the rhizomorph experiences stress greater than its yield stress. Because of the porous nature of the outer layer, stress concentrations form around the edges of the pores. Stress concentrations around ellipses are greatest along the side of the major axis of the ellipse. Under the uniaxial loading, the stress concentrations are greatest on the left and right sides of the pores, along the major axes (Inglis, 1913). When the pores are closer, the magnitude of the stress concentrations between pores becomes larger under the same loading (Jones and Hozos, 1971), (Zhang et al., 2009). The greatest difference in the plastic deformation was a result of varying only the pores in the outside section; When outside pores were a factor of average pore size of 1.12 or greater, the plastic deformation increased to almost three times that of the base case. This indicates that the porosity and pore structure in this section offer the most structural protection. The structure as a whole would be best protected against greater stresses by having a less porous outside section with smaller pores that are further apart, as is the case with the melanized layer of the harvested rhizomorphs (see Figs. 2, 4 and 5). Having larger and nearer pores in the porous layer structure, as

with the cultured rhizomorphs, allows for plastic deformation and then damage, to occur at lower loads than for melanized harvested rhizomorphs. This is demonstrated in Fig. 11, where larger pores resulted in a larger displacement and plastic deformation.

The finite element model and simulations showed a balance between the maximum displacement and plastic deformation of the rhizomorph during loading. With smaller than average pores, there was a smaller maximum displacement (Fig. 11a), though not necessarily a smaller plastic deformation. Both the maximum displacement and the plastic deformation show more dramatic changes with larger than average pores. A factor of average pore size of 1 allowed for the lowest plastic deformation (Fig. 11b) without the increase in maximum displacement found with larger pores. This balance of properties occurs when the size of the pores matches the average size of pores found in harvested rhizomorphs. One benefit of natural materials is the continued reiteration to find the best structure made possible by evolution. The results of the FE model, as seen in Fig. 11, show that the structure of the melanized layer formed by the harvested rhizomorphs, grown in a natural environment, is one that provides for greater protection without damage from mechanical loading. Cultured rhizomorphs, grown in a more controlled environment and lacking the melanized layer, had a structure prone to more permanent deformation and damage under the same loading conditions. This indicates that the uniformity and size of pores produced in a melanized layer are better suited to prevent damage from mechanical loading.

3.6. Properties of the melanized layer

The internal structure of the melanized layer of the harvested rhizomorphs had a radially graded porous structure, with pore areas getting progressively smaller near the outer edge. These smaller pores, especially along the outside of the layer, play an important role in protecting the internal structure, where nutrient and gas transport occur. In addition to protection from mechanical damage, the melanized layer provides chemical protection in the form of calcium, both internally and externally. The presence of calcium in this protective layer not only provides defenses from predation or potential bio-control, but also may help the rhizomorphs to get past host plant defenses. The arrangement of pores in the melanized layer has a distribution that reduces both the maximum deformation and resulting plastic deformation when indented. While a load may attack the outer melanized layer, the pore distribution in that layer minimizes the amount of permanent damage, aiding the resilient structure to continue to infect new hosts. This combination of properties gives novel insight into the resilience of *Armillaria* rhizomorphs and possible avenues that could limit its spread. The melanized layer has likely evolved to protect the inside of the rhizomorph. Experiments used to test new bio-controls that take the protection of the melanized layer into account will have a better understanding of how lab tested treatments will transfer into natural infection sites. By using bio-controls that can break down the melanized layer and directly attack the ability of the rhizomorph to transport essential gasses and nutrients, *Armillaria* infections may be better controlled and contained, saving millions of dollars to those whose crops are affected.

4. Conclusions

The current study used imaging, chemical analysis, mechanical testing, and finite element modeling to understand the defense mechanisms provided by the melanized layer present in *Armillaria ostoyae* rhizomorphs and led to the following conclusions:

- The melanized layer of harvested rhizomorphs had a porous layer, similar to the porous layer of the cultured rhizomorphs that lacked the melanized layer. However, the harvested rhizomorphs layer showed more consistent properties such as porosity, pore

distribution, and hardness values. These results demonstrate that the melanized layer allows for more uniform properties, which strengthens the potential weak spots that could otherwise cause failure and eventually leading to the death of the organism.

- The melanized layer of harvested *Armillaria* rhizomorphs contained a significant amount of calcium in their chemical composition, which was not present in the surface or porous layer of rhizomorphs without a melanized layer. This calcium can provide added defenses against predation, attempted bio-controls, and defense mechanisms used by potential hosts to stop infection.
- The average size of pores, and resulting porosity, found in harvested rhizomorphs provided for the best balance of minimizing the maximum deformation and plastic deformation during mechanical loading, thus providing optimal defense against external mechanical loading.

Author statement

Debora Lyn Porter: Conceptualization, Methodology, Formal Analysis, Investigation, Writing – Original Draft, Writing – Review & Editing, Visualization. **Alexander J. Bradshaw:** Formal Analysis, Investigation, Investigation, Writing – Original Draft. **Ryan H. Nielsen:** Methodology, Software, Validation, Formal Analysis, Writing – Original Draft. **Pania Newell:** Supervision, Resources, Writing – Original Draft. **Bryn T. M. Dentinger:** Supervision, Resources, Writing – Original Draft, Writing – Review & Editing. **Steven E. Naleway:** Project Administration, Funding Acquisition, Writing – Original Draft, Writing – Review & Editing.

Declaration of competing interest

The authors declare that they have no known competing financial interests or personal relationships that could have appeared to influence the work reported in this paper.

Acknowledgments

The authors would like to acknowledge the help of the U.S. Forest service, especially Michael G. McWilliams, in finding and collecting *Armillaria* rhizomorph samples. Additionally, the authors would like to thank Nathan Porter for his help in harvesting rhizomorphs samples.

References

- Adaskaveg, J.E., Förster, H., Wade, L., Thompson, D.F., Connell, J.H., Mar. 1999. Efficacy of sodium Tetrathiocarbonate and propiconazole in managing *Armillaria* root rot of almond on peach rootstock. *Plant Dis.* 83 (3), 240–246. <https://doi.org/10.1094/PDIS.1999.83.3.240>.
- Aguín, O., Mansilla, J.P., Sainz, M.J., 2006. In vitro selection of an effective fungicide against *Armillaria mellea* and control of white root rot of grapevine in the field. *Pest Manag. Sci.* 62 (3), 223–228. <https://doi.org/10.1002/ps.1149>.
- Anderson, J.B., Stasovski, E., 1992. Molecular phylogeny of northern Hemisphere species of *Armillaria*. *Mycologia* 84 (4), 505–516. <https://doi.org/10.2307/3760315>.
- Anderson, J.B., Ullrich, R.C., 1979. Biological species of *Armillaria mellea* in North America. *Mycologia* 71 (2), 402–414. <https://doi.org/10.2307/3759160>.
- Baumgartner, K., Rizzo, D.M., 2001. Distribution of *Armillaria* species in California. *Mycologia* 93 (5), 821–830. <https://doi.org/10.2307/3761748>.
- Baumgartner, K., Rizzo, D.M., Jan. 2002. Spread of *Armillaria* root disease in a California Vineyard. *Am. J. Enol. Vitic.* 53 (3), 197–203.
- Baumgartner, K., Coetzee, M.P.A., Hoffmeister, D., Aug. 2011. Secrets of the subterranean pathosystem of *Armillaria*: Subterranean pathosystem of *Armillaria*. *Mol. Plant Pathol.* 12 (6), 515–534. <https://doi.org/10.1111/j.1364-3703.2010.00693.x>.
- Baumgartner, K., Warnock, A.E., Apr. 2006. A soil inoculant inhibits *Armillaria mellea* in vitro and improves productivity of grapevines with root disease. *Plant Dis.* 90 (4), 439–444. <https://doi.org/10.1094/PD-90-0439>.
- Bergemann, S.E., Garbelotto, M., Sep. 2006. High diversity of fungi recovered from the roots of mature tanoak (*Lithocarpus densiflorus*) in northern California. *Can. J. Bot.* 84 (9), 1380–1394. <https://doi.org/10.1139/b06-097>.
- Coetzee, M.P.A., Wingfield, B.D., Bloomer, P., Ridley, G.S., Wingfield, M.J., 2003. Molecular identification and phylogeny of *Armillaria* isolates from South America and Indo-Malaysia. *Mycologia* 95 (2), 285–293. <https://doi.org/10.2307/3762039>.

- Coetzee, M.P.A., Wingfield, B.D., Wingfield, M.J., Oct. 2018. *Armillaria* root-rot pathogens: species boundaries and global distribution. *Pathogens* 7 (4). <https://doi.org/10.3390/pathogens7040083>.
- Cordero, R.J.B., Casadevall, A., Mar. 2017. Functions of fungal melanin beyond virulence. *Fungal Biol. Rev.* 31 (2), 99–112. <https://doi.org/10.1016/j.fbr.2016.12.003>.
- Cox, K.D., Scherm, H., Jun. 2006. Interaction dynamics between saprobic lignicolous fungi and *Armillaria* in controlled environments: exploring the potential for competitive exclusion of *Armillaria* on peach. *Biol. Control* 37 (3), 291–300. <https://doi.org/10.1016/j.biocontrol.2006.01.012>.
- DeLong, R.L., Lewis, K.J., Simard, S.W., Gibson, S., Dec. 2002. Fluorescent pseudomonad population sizes baited from soils under pure birch, pure Douglas-fir, and mixed forest stands and their antagonism toward *Armillaria ostryae* in vitro. *Can. J. For. Res.* 32 (12), 2146. <https://doi.org/10.1139/x02-141>.
- Dentinger, B.T.M., Didukh, M.Y., Moncalvo, J.-M., Sep. 2011. Comparing COI and ITS as DNA barcode markers for mushrooms and allies (agaricomycotina). *PLoS One* 6 (9). <https://doi.org/10.1371/journal.pone.0025081> e25081–e25081.
- Erko, M., Hartmann, M.A., Zlotnikov, I., Valverde Serrano, C., Fratzl, P., Politi, Y., Aug. 2013. Structural and mechanical properties of the arthropod cuticle: comparison between the fang of the spider *Cupiennius salei* and the carapace of American lobster *Homarus americanus*. *J. Struct. Biol.* 183 (2), 172–179. <https://doi.org/10.1016/j.jsb.2013.06.001>.
- Ferguson, B.a., Dreisbach, T.a., Parks, C.g., Flip, G.m., Schmitt, C.l., Apr. 2003. Coarse-scale population structure of pathogenic *Armillaria* species in a mixed-conifer forest in the Blue Mountains of northeast Oregon. *Can. J. For. Res.* 33 (4), 612. <https://doi.org/10.1139/x03-065>.
- Fogarty, R.V., Tobin, J.M., Sep. 1996. Fungal melanins and their interactions with metals. *Enzym. Microb. Technol.* 19 (4), 311–317. [https://doi.org/10.1016/0141-0229\(96\)00002-6](https://doi.org/10.1016/0141-0229(96)00002-6).
- Gardes, M., Bruns, T.D., Apr. 1993. ITS primers with enhanced specificity for basidiomycetes—application to the identification of mycorrhizae and rusts. *Mol. Ecol.* 2 (2), 113–118. <https://doi.org/10.1111/j.1365-294x.1993.tb00005.x>.
- Grillo, R., Korhonen, K., Hantula, J., Hietala, A.M., Jul. 2000. Genetic evidence for Somatic Haplodization in developing fruit bodies of *Armillaria tabescens*. *Fungal Genet. Biol.* 30 (2), 135–145. <https://doi.org/10.1006/fgbi.2000.1213>.
- Inglis, C.E., 1913. Stresses in plates due to the presence of cracks and sharp corners. *Trans. Inst. Nav. Archit.* 55, 219–241.
- Jones, N., Hozos, D., May 1971. A study of the stresses around elliptical holes in flat plates. *J. Eng. Ind.* 93 (2), 688–694. <https://doi.org/10.1115/1.3427982>.
- Koch, R.A., Wilson, A.W., Séné, O., Henkel, T.W., Aime, M.C., Jan. 2017. Resolved phylogeny and biogeography of the root pathogen *Armillaria* and its gasteroid relative, *Guyanagaster*. *BMC Evol. Biol.* 17 (1), 33. <https://doi.org/10.1186/s12862-017-0877-3>.
- Kromroy, K.W., Blanchette, R.A., Grigal, D.F., Jun. 2005. *Armillaria* species on small woody plants, small woody debris, and root fragments in red pine stands. *Can. J. For. Res.* 35 (6), 1487–1495. <https://doi.org/10.1139/X05-067>.
- Lofaj, F., Németh, D., Nov. 2017. Multiple cohesive cracking during nanoindentation in a hard W-C coating/steel substrate system by FEM. *J. Eur. Ceram. Soc.* 37 (14), 4379–4388. <https://doi.org/10.1016/j.jeurceramsoc.2017.03.051>.
- Mihail, J.D., Bruhn, J.N., Nov. 2005. Foraging behaviour of *Armillaria* rhizomorph systems. *Mycol. Res.* 109 (11), 1195–1207. <https://doi.org/10.1017/S0953756205003606>.
- Munnecke, D.E., Nov. 1973. Effect of A soil microflora selected by carbon disulphide fumigation on survival of *Armillaria mellea* in woody host tissues. *Phytopathology* 63 (11), 1352–1357. <https://doi.org/10.1139/m57-018>.
- Munnecke, D.E., May 1981. Interactions involved in controlling *Armillaria mellea*. *Plant Dis.* 65 (5), 384–389. <https://doi.org/10.1094/pd-65-384>.
- Nagy, N.E., et al., Oct. 2012. The pathogenic white-rot fungus *Heterobasidion parvirosum* responds to Spruce Xylem defense by enhanced production of oxalic acid. *Mol. Plant Microbe Interact.* 25 (11), 1450–1458. <https://doi.org/10.1094/MPMI-02-12-0029-R>.
- Naleway, S.E., Porter, M.M., McKittrick, J., Meyers, M.A., Oct. 2015. Structural Design elements in biological materials: application to bioinspiration. *Adv. Mater.* 27 (37), 5455–5476. <https://doi.org/10.1002/adma.201502403>.
- Nicolás-Bermúdez, J., Arzate-Vázquez, I., Chanona-Pérez, J.J., Méndez-Méndez, J.V., Rodríguez-Castro, G.A., Martínez-Gutiérrez, H., Nov. 2018. Morphological and micromechanical characterization of calcium oxalate (CaOx) crystals embedded in the pecan nutshell (*Carya illinoensis*). *Plant Physiol. Biochem.* 132, 566–570. <https://doi.org/10.1016/j.plaphy.2018.10.008>.
- Oliver, W.C., Pharr, G.M., Jun. 1992. An improved technique for determining hardness and elastic modulus using load and displacement sensing indentation experiments. *J. Mater. Res.* 7 (6), 1564–1583. <https://doi.org/10.1557/JMR.1992.1564>.
- Ota, Y., Fukuda, K., Suzuki, K., 1998. The Nonheterothallic life cycle of Japanese *Armillaria mellea*. *Mycologia* 90 (3), 396–405. <https://doi.org/10.2307/3761398>.
- Pellegrini, A., Prodrutti, D., Pertot, I., Oct. 2014. Use of bark mulch pre-inoculated with *Trichoderma atroviride* to control *Armillaria* root rot. *Crop Protect.* 64, 104–109. <https://doi.org/10.1016/j.cropro.2014.06.007>.
- Pildain, M.B., Coetzee, M.P.A., Wingfield, B.D., Wingfield, M.J., Rajchenberg, M., 2010. Taxonomy of *Armillaria* in the patagonian forests of Argentina. *Mycologia* 102 (2), 392–403.
- Proffer, T.J., 1987. Biological species of *Armillaria* isolated from Sour cherry orchards in Michigan. *Phytopathology* 77 (6), 941. <https://doi.org/10.1094/Phyto-77-941>.
- Qin, G.-F., Zhao, J., Korhonen, K., 2007. A study on Intersterility groups of *Armillaria* in China. *Mycologia* 99 (3), 430–441.

- Rizzo, D.M., Blanchette, R.A., Palmer, M.A., Aug. 1992. Biosorption of metal ions by *Armillaria rhizomorpha*. *Can. J. Bot.* 70 (8), 1515–1520. <https://doi.org/10.1139/b92-190>.
- Sanati Nezhad, A., Geitmann, A., Nov. 2013. The cellular mechanics of an invasive lifestyle. *J. Exp. Bot.* 64 (15), 4709–4728. <https://doi.org/10.1093/jxb/ert254>.
- Schnabel, G., Bryson, P.K., Williamson, M.A., Aug. 2006. First report of *Armillaria tabescens* causing *Armillaria* root rot of pindo palm in South Carolina. *Plant Dis.* 90 (8) <https://doi.org/10.1094/PD-90-1106A>, 1106–1106.
- Schoch, C.L., et al., Apr. 2012. Nuclear ribosomal internal transcribed spacer (ITS) region as a universal DNA barcode marker for Fungi. *Proc. Natl. Acad. Sci. Unit. States Am.* 109 (16), 6241–6246. <https://doi.org/10.1073/pnas.1117018109>.
- Sipos, G., et al., Dec. 2017. Genome expansion and lineage-specific genetic innovations in the forest pathogenic fungi *Armillaria*. *Nat. Ecol. Evol.* 1 (12) <https://doi.org/10.1038/s41559-017-0347-8>. Art. no. 12.
- Torres-Torres, D., Muñoz-Saldaña, J., Guevara, L.A.G.-L., Hurtado-Macías, A., Swain, M. V., Sep. 2010. Geometry and bluntness tip effects on elastic–plastic behaviour during nanoindentation of fused silica: experimental and FE simulation. *Model. Simulat. Mater. Sci. Eng.* 18 (7) <https://doi.org/10.1088/0965-0393/18/7/075006>, 075006.
- Tremble, K., Suz, L.M., Dentinger, B.T.M., Jul. 2020. Lost in translation: population genomics and long-read sequencing reveals relaxation of concerted evolution of the ribosomal DNA cistron. *Mol. Phylogenet. Evol.* 148, 106804. <https://doi.org/10.1016/j.ympev.2020.106804>.
- Ullrich, R.C., Anderson, J.B., Jun. 1978. Sex and diploidy in *Armillaria mellea*. *Exp. Mycol.* 2 (2), 119–129. [https://doi.org/10.1016/S0147-5975\(78\)80025-5](https://doi.org/10.1016/S0147-5975(78)80025-5).
- Wallander, H., Mahmood, S., Hagerberg, D., Johansson, L., Pallon, J., 2003. Elemental composition of ectomycorrhizal mycelia identified by PCR–RFLP analysis and grown in contact with apatite or wood ash in forest soil. *FEMS Microbiol. Ecol.* 44 (1), 57–65. <https://doi.org/10.1111/j.1574-6941.2003.tb01090.x>.
- Wan, C., Hao, Z., Jun. 2020. Natural arrangement of micro-strips reduces shear strain in the locust cuticle during power amplification. *J. Biomech.* 107, 109842. <https://doi.org/10.1016/j.jbiomech.2020.109842>.
- West, J.S., Fox, R.T.V., 2002. Stimulation of *Armillaria mellea* by phenolic fungicides. *Ann. Appl. Biol.* 140 (3), 291–295. <https://doi.org/10.1111/j.1744-7348.2002.tb00184.x>.
- White, T.J., Bruns, T., Lee, S., Taylor, J., 1990. Amplification and direct sequencing of fungal ribosomal RNA genes for phylogenetics. In: Innis, M.A., Gelfand, D.H., Sninsky, J.J., White, T.J. (Eds.), *PCR Protocols: a Guide To Methods and Applications*. Academic Press, Orlando, pp. 315–322. <https://doi.org/10.1016/B978-0-12-372180-8.50042-1>.
- Whitney, K.D., Arnott, H.J., 1987. Calcium oxalate crystal morphology and development in *agaricus bisporus*. *Mycologia* 79 (2), 180–187. <https://doi.org/10.2307/3807650>.
- D. Wilson, M. Olmstead, and G. Schnabel, “*Armillaria* root rot,” *RosBREED*. <https://www.rosbreed.org/rosaceae-nemesis/armillaria> (accessed Dec. 17, 2020).
- Yafetto, L., 2018. The structure of mycelial cords and rhizomorphs of fungi: a minireview. *Mycosphere* 9 (5), 984–998. <https://doi.org/10.5943/mycosphere/9/5/3>.
- Yafetto, L., Davis, D.J., Money, N.P., Sep. 2009. Biomechanics of invasive growth by *Armillaria* rhizomorphs. *Fungal Genet. Biol.* 46 (9), 688–694. <https://doi.org/10.1016/j.fgb.2009.04.005>.
- Yahr, R., Schoch, C.L., Dentinger, B.T.M., Sep. 2016. Scaling up discovery of hidden diversity in fungi: impacts of barcoding approaches. *Philos. Trans. R. Soc. Lond. B Biol. Sci.* 371 (1702) <https://doi.org/10.1098/rstb.2015.0336>.
- Yang, W., et al., Aug. 2014. Protective role of *Arapaima gigas* fish scales: structure and mechanical behavior. *Acta Biomater.* 10 (8), 3599–3614. <https://doi.org/10.1016/j.actbio.2014.04.009>.
- Yu, H.Q., Jiang, Z.H., Hse, C.Y., Shupe, T.F., 2008. Selected physical and mechanical properties of moso bamboo (*Phyllostachys pubescens*). *J. Trop. For. Sci.* 20 (4), 258–263.
- Zabka, M., Pavela, R., Oct. 2013. Antifungal efficacy of some natural phenolic compounds against significant pathogenic and toxinogenic filamentous fungi. *Chemosphere* 93 (6), 1051–1056. <https://doi.org/10.1016/j.chemosphere.2013.05.076>.
- Zhang, L.Q., Lu, A.Z., Yue, Z.Q., Yang, Z.F., Jan. 2009. An efficient and accurate iterative stress solution for an infinite elastic plate around two elliptic holes, subjected to uniform loads on the hole boundaries and at infinity. *Eur. J. Mech. - ASolids* 28 (1), 189–193. <https://doi.org/10.1016/j.euromechsol.2008.04.003>.
- Hysitron probe Part Specifications. Bruker, Dec. 07, 2016.
- Hysitron probe selection guide. Bruker, 2015. Accessed: Nov. 04, 2020. [Online]. Available: https://cpb-us-w2.wpmucdn.com/sites.gatech.edu/dist/5/361/files/2016/07/Hysitron_Probe_Selection_Guide-2015-probou-rlf.pdf.